High Capacity and Efficiency Optimization of Compressive Antennas for Imaging Applications

Richard Obermeier[1], Jose Angel Martinez-Lorenzo[1,2]
[1]Electrical & Computer Engineering, Northeastern University, Boston, MA, USA
[2]Mechanical & Industrial Engineering, Northeastern University, Boston, MA, USA
jmartinez@coe.neu.edu

***Abstract*—Compressive Reflector Antennas (CRA) have been shown to provide enhanced imaging capabilities over Traditional Reflector Antennas (TRA) when compressed sensing (CS) techniques are employed. This paper presents a novel method for designing dielectric CRA's for high sensing capacity imaging applications. In the design procedure, the dielectric constants of scatterers added to a TRA are optimized in order to maximize the capacity and efficiency of the imaging system's sensing matrix. Numerical results are presented that demonstrate the method's ability to enhance the CS reconstruction capabilities of the CRA.**

***Index Terms*—compressive sensing, antenna design, coded apertures**

I. Introduction

Compressive reflector antennas (CRA) [1]–[3] are a class of antennas specifically designed for high capacity sensing and imaging applications. CRA's operate in a manner similar to that of the coded apertures utilized in optical imaging applications [4]–[6]: by introducing scatterers to the surface of a traditional reflector antenna (TRA), the compressive antenna encodes a pseudo-random phase front on the scattered electric field. It was shown in [1] that, by modifying the encoded wavefront from measurement to measurement, compressive sensing (CS) techniques [7]–[9] can be employed in imaging applications with improved performance over the TRA.

In [3], a numerical design method for compressive antennas was developed based on the notion that en-

II. Motivation

Consider a general linear system, in which a set of noisy measurements $\mathbf{y} \in \mathbb{C}^M$ of the object of interest $\boldsymbol{x} \in \mathbb{C}^N$ are obtained via the relationship $\mathbf{y} = \mathbf{A}\boldsymbol{x} + \mathbf{n}$, where $\mathbf{A} \in \mathbb{C}^{M\times N}$ is called the sensing matrix. When $M < N$, there are an infinite number of solutions $\mathbf{x}$ satisfying $\mathbf{y} = \mathbf{A}\boldsymbol{x}$, and so regularization techniques must be employed in order to generate a unique solution. A particularly interesting scenario arises when the vector $\boldsymbol{x}$ is sparse, i.e. the number of non-zero elements S in $\boldsymbol{x}$ is much smaller than the total number of elements N. In this case, compressive sensing theory [7]–[9] establishes that the sparse vector can be recovered from an incomplete set of measurements as the solution to the following convex optimization program:

$$\begin{aligned} \underset{\boldsymbol{x}}{\text{minimize}} \quad & \|\boldsymbol{x}\|_{\ell_1} \\ \text{subject to} \quad & \|\mathbf{A}\boldsymbol{x} - \mathbf{y}\|_{\ell_2} \leq \eta \end{aligned} \tag{1}$$

Accurate reconstruction is only guaranteed when the sensing matrix satisfies the requirements of a suitable metric. One such metric, the Restricted Isometry Property (RIP), uses the notion of restricted isometry constants: for a fixed sparsity level S, the restricted isometry constant δ_S is the smallest positive constant such that

$$(1-\delta_S)\|\mathbf{x}\|_{\ell_2}^2 \leq \|\mathbf{A}\mathbf{x}\|_{\ell_2}^2 \leq (1+\delta_S)\|\mathbf{x}\|_{\ell_2}^2 \tag{2}$$

is satisfied for all vectors with $\|\mathbf{x}\|_{\ell_0} \leq S$, where the "$\ell_0-$norm" measures the number of non-zero elements

In [3], the sensing capacity for the complete matrix A was shown to establish the following lower bound for the restricted isometry constants δ_S:

$$\delta_S \geq 1 - 2^{2H_1(\blacksquare)} = 1 - \prod_{m=1}^{M} \sigma_m^2 \tag{4}$$

By increasing the sensing capacity, the lower bound for the restricted isometry constants is improved, thereby improving the likelihood that compressive sensing techniques will be successful.

III. Design Method

A. Capacity Maximization Problem

Consider an electromagnetic sensing system that utilizes several transmitting and receiving antennas. The fields radiated by the transmitting antenna on the m-th measurement can be denoted by the vector $\mathbf{g}_{t,i,m} \in \mathbb{C}^N$, where $i = 1, 2, 3$ denotes the component of the electric field and N denotes the number of points in the imaging region. Similarly, the radiation pattern of the receiving antenna on the m-th measurement can be denoted by the vector $\mathbf{g}_{r,i,m} \in \mathbb{C}^N$. By concatenating the radiated fields for all M measurements, we can formulate the field matrices $\mathbf{G}_{t,i}, \mathbf{G}_{r,i} \in \mathbb{C}^{M \times N}$. According to the reciprocity theorem, the sensing matrix $\mathbf{A} \in \mathbb{C}^{M \times N}$ can be expressed as $\mathbf{A} = \sum_{i=1}^{3} \zeta \left(\mathbf{G}_{r,i} \odot \mathbf{G}_{t,i} \right)$, where ζ is a positive scaling constant and $\odot$ is the Hadamard (element-wise) product. This is an instance of the Born approximation.

Suppose that the radiated fields can be expressed as a function of design variables $\boldsymbol{x} \in \mathbb{R}^P$. The unified design problem seeks the optimal solution to the following non-convex optimization program:

$$\begin{aligned} \underset{\boldsymbol{x}}{\text{maximize}} \quad & \alpha \log\det\left(\mathbf{A}(\boldsymbol{x})\mathbf{A}^H(\boldsymbol{x}) + \beta \mathbf{I}_M\right) \\ & + \sum_{m=1}^{M} \mathbf{a}_m(\boldsymbol{x}) \mathbf{\Lambda}_m \mathbf{a}_m^H(\boldsymbol{x}) \\ \text{subject to} \quad & \boldsymbol{x} \in Q_p \end{aligned} \tag{5}$$

where $\mathbf{a}_m$ is the $m-$th row of the sensing matrix. The coefficients α and Λ_m are used to weigh the capacity and quadratic terms. If all Λ_m are equal

the background medium whose Green's functions are known, MECA can compute the electric and magnetic fields at any position.

The computational efficiency of MECA makes it a more suitable forward model for designing dielectric CRA's than full-wave methods, such as the Finite Difference in the Frequency Domain (FDFD) method [12]. In the dielectric CRA design problem, the $i-$th component of the electric field radiated by antenna a (replace with t for a transmitter, r for a receiver) on the $m-$th measurement can be expressed as follows:

$$\begin{aligned} \mathbf{g}_{a,i,m}(\boldsymbol{x}) = \mathbf{e}_{a,i,m} &+ \mathbf{E}_{TE,a,i,m} \mathbf{\Gamma}_{TE,a,m}(\boldsymbol{x}) \\ &+ \mathbf{E}_{TM,a,i,m} \mathbf{\Gamma}_{TM,a,m}(\boldsymbol{x}) \end{aligned} \tag{6}$$

where $\boldsymbol{x} \in \mathbb{R}^P$ are the dielectric constants of the scatterers at each triangular facet, $\mathbf{e}_{a,i,m} \in \mathbb{C}^N$ is the direct-path radiation from the antenna to the imaging region, $\mathbf{E}_{TE,a,i,m}, \mathbf{E}_{TM,a,i,m} \in \mathbb{C}^{N \times P}$ are the TE and TM "Green's functions", and $\mathbf{\Gamma}_{TE,a,m}(\boldsymbol{x}), \mathbf{\Gamma}_{TM,a,m}(\boldsymbol{x}) \in \mathbb{C}^P$ are the reflection coefficients of each scatterer. The reflection coefficients are computed by treating each facet of the CRA as a three-layer medium containing the background medium (i.e. freespace), the dielectric scatterer, and the perfect electric conductor (PEC) reflector. MECA considers the incident fields to be locally planar at each facet, such that the reflection coefficient of the $p-$th scatterer can be expressed as follows:

$$\begin{aligned} \Gamma_{m,p}(\epsilon_p) = \Gamma_{bp,m}(\epsilon_p) &\\ - \frac{T_{bp,m}(\epsilon_p) T_{pb,m}(\epsilon_p) e^{-\jmath 2\phi_{\blacksquare\blacksquare}(\epsilon_{\blacksquare})}}{1 + \Gamma_{pb,m}(\epsilon_p) e^{-\jmath 2\phi_{\blacksquare\blacksquare}(\epsilon_{\blacksquare})}} & \end{aligned} \tag{7}$$

$$\phi_{m,p}(\epsilon_p) = 2\pi f_m \sqrt{\mu_0 \epsilon_0 \epsilon_p} d_p \cos(\theta_{t_{\blacksquare} m,p}(\epsilon_p)) \tag{8}$$

where $\Gamma_{bp,m}(\epsilon_p)$ and $T_{bp,m}(\epsilon_p)$ are the half-plane reflection and transmission coefficients going from the background medium to the dielectric, $\Gamma_{pb,m}(\epsilon_p)$ and $T_{pb,m}(\epsilon_p)$ are the half-plane reflection and transmission coefficients going from the dielectric to the background medium, f_m is the frequency, d_p is the thickness of the dielectric, and $\theta_{t_{\blacksquare} m,p}(\epsilon_p)$ is the angle of propagation in the dielectric. Note that we have replaced the generic design variable x_p with the dielectric constant ϵ_p for clarity. Eq. 7 is a simplified version of the general relationship described in [13]

ten frequencies uniformly spaced between 70.5[GHz] and 77[GHz], for a total of 160 measurements. The antennas were modeled as horn antennas, wherein the electric field was oriented in the $+z$ direction and the direction of propagation was the $-x$ direction. The parabolic CRA reflector, which was located at $x = -0.5$[m], was discretized into 3750 triangular facets. The design procedure was configured to optimize the dielectric constant of each triangular facet, wherein $\epsilon_r \in [1, 30]$. All dielectrics had the same thickness $d = 8.13$[mm], which is approximately two times the average wavelength of the operating frequencies. The imaging region consisted of 625 positions uniformly spaced along a 0.2[m] $\times$ 0.2[m] grid centered at $x = 0.9$[m]. The problem was configured to optimize only the capacity of the sensing matrix by setting $\alpha = 1$ and $\Lambda_m = 0 \; \forall \; m \in 1, \ldots, M$. To initialize the optimization procedure, the starting dielectric constant values were randomly selected over the feasible set.

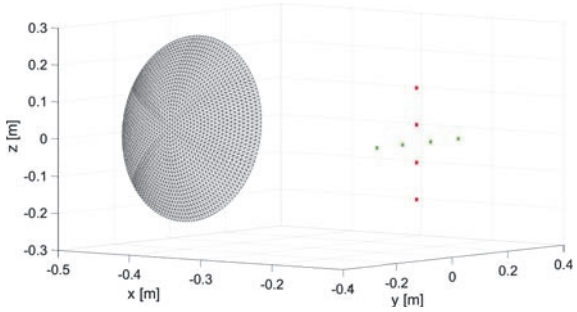

Fig. 1. Test configuration for the design problem. Four transmitting (green dots) and four receiving antennas (red dots) were used in conjunction with the dielectric CRA reflector located at $x = -0.5$[m].

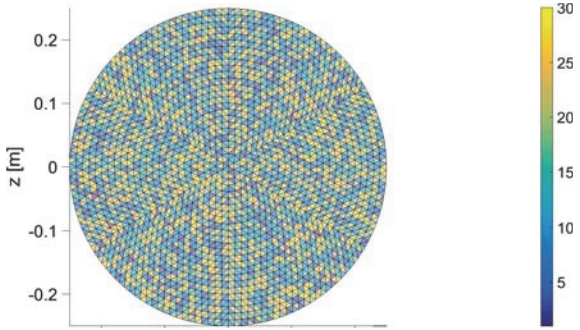

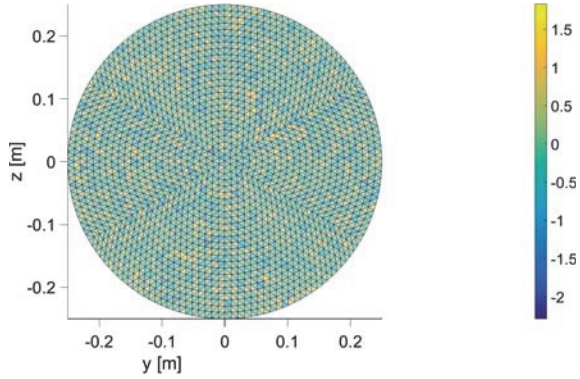

Fig. 3. Difference in dielectric constant between the optimized CRA and the baseline randomized CRA.

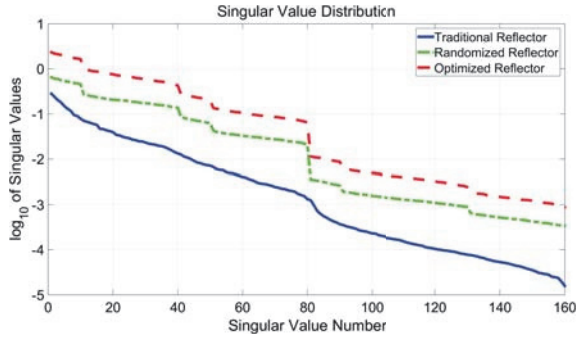

Fig. 4. Singular values of the sensing matrices obtained using the TRA, baseline randomized CRA, and optimized CRA.

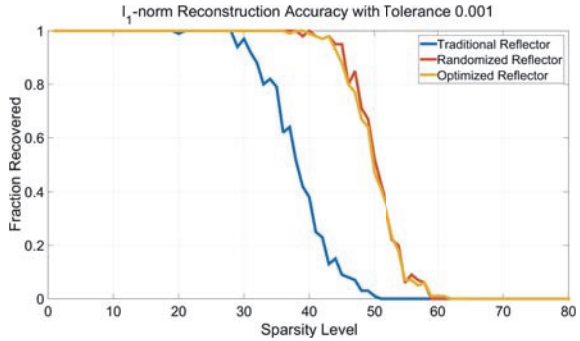

Fig. 5. Numerical comparison of the reconstruction accuracies of ℓ_1-norm minimization using the sensing matrices obtained using the TRA, baseline randomized CRA, and optimized CRA.

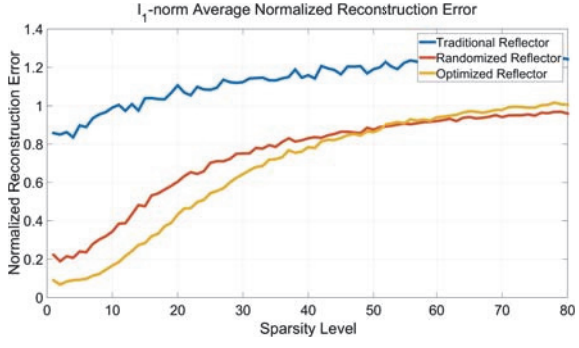

Fig. 6. Numerical comparison of the reconstruction accuracies of ℓ_1-norm minimization using the sensing matrices obtained using the TRA, baseline randomized CRA, and optimized CRA.

when the measurements are corrupted by noise due to its enhanced capacity. The first and second items are confirmed for this design scenario by Figure 5, which display the ℓ_1-norm reconstruction capabilities of all three CRA's in the noiseless scenario. The third item is confirmed by Figure 6, which displays the ℓ_1-norm reconstruction capabilities of all three CRA's in the presence of noise.

V. Conclusion

This paper describes a novel method for designing dielectric CRA's for high sensing capacity imaging applications. Unlike the previous design methods, the design method presented in this paper properly considers the coupling between the transmitting and receiving antennas. The method was assessed for a parabolic CRA that utilized four transmitting antennas and four receiving antennas in a multiple-monostatic configuration. A numerical analysis of reconstruction accuracy demonstrated the design method's ability to generate CRA's with enhanced CS reconstruction capabilities.

ACKNOWLEDGEMENT

This work has been partially funded by NSF CAREER program (Award No. 1653671) and the U.S. Department of Homeland Security (Award No. 2013-ST-061-ED0001).

[5] G. D. De Villiers, N. T. Gordon, D. A. Payne, I. K. Proudler, I. D. Skidmore, K. D. Ridley, C. R. Bennett, R. A. Wilson, and C. W. Slinger, "Sub-pixel super-resolution by decoding frames from a reconfigurable coded-aperture camera: theory and experimental verification," in *SPIE Optical Engineering+ Applications*. International Society for Optics and Photonics, 2009, pp. 746 806–746 806.

[6] R. F. Marcia and R. M. Willett, "Compressive coded aperture superresolution image reconstruction," in *Acoustics, Speech and Signal Processing, 2008. ICASSP 2008. IEEE International Conference on*. IEEE, 2008, pp. 833–836.

[7] E. J. Candès, J. Romberg, and T. Tao, "Robust uncertainty principles: Exact signal reconstruction from highly incomplete frequency information," *Information Theory, IEEE Transactions on*, vol. 52, no. 2, pp. 489–509, 2006.

[8] E. J. Candes, J. K. Romberg, and T. Tao, "Stable signal recovery from incomplete and inaccurate measurements," *Communications on pure and applied mathematics*, vol. 59, no. 8, pp. 1207–1223, 2006.

[9] D. L. Donoho, "Compressed sensing," *Information Theory, IEEE Transactions on*, vol. 52, no. 4, pp. 1289–1306, 2006.

[10] M. D. Migliore, "On electromagnetics and information theory," *Antennas and Propagation, IEEE Transactions on*, vol. 56, no. 10, pp. 3188–3200, 2008.

[11] M. D. Migliore and D. Pinchera, "Compressed sensing in electromagnetics: Theory, applications and perspectives," in *Antennas and Propagation (EUCAP), Proceedings of the 5th European Conference on*. IEEE, 2011, pp. 1969–1973.

[12] C. Rappaport, A. Morgenthaler, and M. Kilmer, "FDFD modeling of plane wave interactions with buried objects under rough surfaces,," in *2001 IEEE Antenna and Propagation Society International Symposium*, 2001, p. 318.

[13] W. C. Chew, *Waves and Fields in Inhomogeneous Media*. IEEE Press, 1995.